

<sup>1\*</sup>T Eswara Rao  
<sup>2</sup>S Srinivasa Rao  
<sup>3</sup>J Ankamma Rao  
<sup>4</sup>B Trinadha  
<sup>5</sup>P Guruvulu  
 Naidu  
<sup>6</sup>Vakada Krishna  
<sup>7</sup>P Bharat Kumar  
<sup>8</sup>B Naidu

## Real time Implementation of PV- Wind Hybrid System using FPGA- MPPT Controller



**Abstract:** A photovoltaic (PV), wind and battery-based hybrid system is proposed in this study. A PV system is implemented using mathematical analysis to improve the performance of the PV system, and a DC-DC boost converter is proposed. Different maximum power point tracking (MPPT) techniques are implemented in this paper to obtain the maximum power from the PV system. A doubly-fed induction generator (DFIG)-based wind emulator was used to design a wind energy system that could operate at all speeds. Suitable control techniques were designed for both rotor-side and grid-side converters of the DFIG system. The required reference signal for pulse width modulation (PWM) controllers is taken from the system currents and converted to two-phase coordinates, that is, direct and quadrature axis models. An IGBT-based bidirectional converter with a battery system is designed for energy storage. To maintain proper synchronization between DG systems and the grid, a PWM-based controller is implemented for a three-phase inverter, which also helps mitigate power-quality distortions. The proposed hybrid system was implemented in real-time hardware with a PV of 1 kW and a wind system of 1.5 kW. The algorithms of the MPPT techniques, such as perturb and observe (P&O) and incremental conductance (INC), were implemented in a field-programmable gate array (FPGA) controller. This study proposes a power management strategy for the proposed hybrid system using P&O and INC algorithms under different load conditions. A comparative analysis of the total harmonic distortion (THD) was performed using an current control technique in the hardware setup.

**Keywords:** Grid Connected PV system; PV-wind hybrid system; Perturb & Observe (PO); INC MPPT; Boost converter; DFIG; Battery.

### I. INTRODUCTION

Renewable energy sources are not emptied when the energy is harnessed. The human use of renewable energy requires technologies that harness natural phenomena, such as sunlight, wind, waves, water flow, and geothermal heat. Among the above-mentioned sources of energy, there has been considerable technological development to harness energy from wind and sunlight, which are abundantly available in nature [1]. A wind and PV system with a battery storage hybrid topology has been proposed, which makes uses a depicted boost-type DC-DC converter for solar PV systems, bidirectional converters for battery systems, and back-to-back converters for double-fed induction generator (DFIG) systems, which are meant to generate voltage levels according to the grid requirements of the PV system [2]. The solar power generation system is optimized by opting for closed-loop algorithms to track the maximum power, and the ever-varying output of the solar collectors is brought to a constant value with the help of the DC-DC converter system, which uses a closed-loop approach to vary the duty cycle of the switching device based on the sensed value of the panel output voltage [3]. Generally, the efficiency of a wind system is improved with the help of an efficient turbine design, mechanical coupling, speed control, and generating systems. The choice of the turbine is very important because it determines parameters such as tip speed ratio (TSR), conversion efficiency, and cut-in speed [4,5]. The speed of turbine rotation completely depends on the design and characteristics of the wind, and the turbine speed should not vary significantly with respect to the rated speed because it affects the generation characteristics [6,7]. In this study, the performance analysis of DFIG in various modes of operation and their power-sharing among all its components, as well as the power management strategy of solar, wind, and battery power using different MPPT algorithms, as well as power quality issues, such as the total harmonic distortion (THD) of the grid current [8].

<sup>1,4</sup> Vignan's Institute of Information Technology (A), Duvvada, Visakhapatnam

<sup>2</sup>Gitam deemed to be university, Visakhapatnam.

<sup>3</sup>Assosa University, Ethiopia.

<sup>5</sup>Aditya Institute of Technology and Management, Tekkali.

<sup>6,7,8</sup>Vignan's Institute of Engineering for Women (A), Duvvada, Visakhapatnam.

Corresponding author: Thamatapu Eswara Rao, Associate Professor, Vignan's Institute of Information Technology.

Email: eswareee@vignaniit.edu.in

Copyright © JES 2024 on-line : journal.esrgroups.org

## II. GRID CONNECTED PV SYSTEM

The proposed grid-connected PV system with a conventional DC-DC converter is shown in Fig.1. The proposed PV system was designed as a distributed energy source because it is freely available in nature and is highly efficient [9]. Because of these parameters, PV systems play a key role in power systems. As per the block diagram, the solar PV output is given to the boost converter, which is controlled by a field-programmable gate array controller for the MPPT. This is boosted by the bidirectional converter from the battery voltage because the voltage coming from the battery is 144 V, but the bus voltage is 300 V. Therefore, to match the bus voltage, a bidirectional converter is used, and the voltage source converter (VSC) converts the DC supply to an AC supply and is supplied to the grid [10]. The PV system parameters are listed in Table 1.

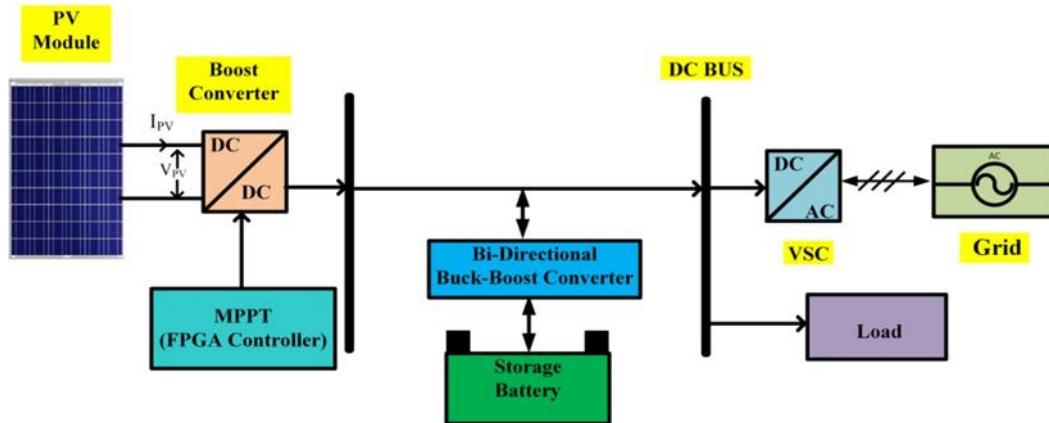


Fig.1. System Architecture of Proposed PV Grid-connected system

Table 1. System Parameters for PV System.

Parameter Variable	Value
<b>Maximum Power</b>	100W
<b>voltage at max Power</b>	18.7V
<b>Current at max Power</b>	5.35A
<b>Open Circuit Voltage</b>	22.32V
<b>Short Circuit Current</b>	5.65A
<b>No. of panels</b>	10
<b>No. of strings</b>	1
<b>Type of cell</b>	Polycrystalline silicon

## III. DC-DC CONVERTERS

DC-DC power converters are employed in various applications, including power supplies for personal computers, office equipment, spacecraft power systems, laptops, telecommunication equipment, and drives. A DC converter can be considered as a DC equivalent to an AC transformer with a continuously variable turn ratio. Similar to a transformer, it can be used to step up or down a DC voltage source [11].

### A. Boost Converter

An MPPT based DC-DC converter was used to improve the efficiency of the PV system, as shown in Fig.2. The purpose of MPPT is to generate a suitable reference signal for a boost converter based on the PV system parameters. The boost converter specifications are presented in Table 2. Here, P&O and INC were chosen as MPPT controllers. To maintain proper equilibrium between the PV and grid systems, a PWM-based inverter was proposed. From the boost converter, the output power is provided to the DC bus, where the load that handles the DC power can be directly connected to the DC bus [12]. A bidirectional converter is used to interface the DC variables comprising the DC/AC conversion, which helps to convert the generated power from the solar PV array to an alternate current that can be further supplied to the grid. A field-programmable gate array is an integrated circuit that is designed according to the requirements of the control unit. Generally, an FPGA is specified as a hardware description language similar to that used for application-specified integrated circuits and provides the necessary information required to the FPGA controller to maintain a flexible constant outcome to the grid. The FPGA controller provides gate pulses to the bidirectional converter, which helps the device trigger a respectable moment for an effective voltage [13].

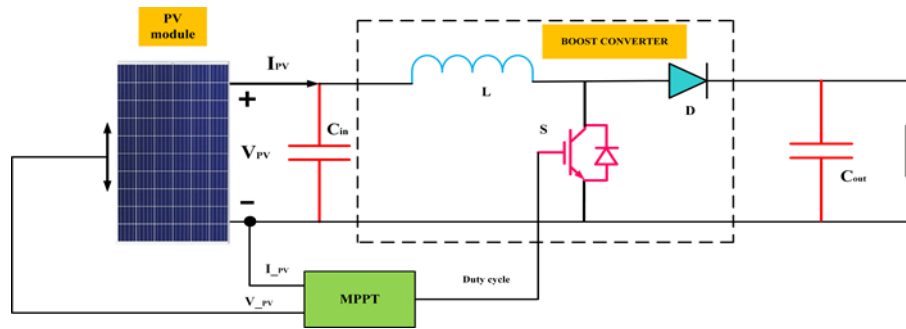


Fig.2. Hardware Implementation for Boost Converter.

Table 2. DC-DC Boost converter Specifications

Parameter Variable	Value
Output Power	20KVA
Input DC-Link Voltage	350V
DC-Link Capacitor	660μF/450Vdc
Switching Frequency up to	100KHz
Output Frequency	10-50Hz
Load Current	15A Peak
IGBT	1200V/100A

Table.3. Parameters of Back-to-Back converters

Parameter Variable	Value
Output Power	1500W
Input Voltage Range DC(Min)	150V
O/P voltage range DC (Max)	350V
Switching Frequency up to	100KHz
Inductor(L)	5mH
Capacitors (C <sub>in</sub> & C <sub>out</sub> )	1500μF
IGBT	1200V/100A

**B. Double Fed Induction Generator (DFIG)**

There are two types of induction motors: asynchronous and synchronous motors. We used an asynchronous motor called the slip-ring induction motor (SRIM). A slip-ring induction motor with a back-to-back converter configuration is called a double-fed induction generator [14]. The proposed DFIG circuit is shown in Fig.3. The rotor of a slip-ring induction motor connected to a converter is called the rotor-side converter (RSC). In this DFIG, the supply is provided to the rotor, and because of the induction principle, the output power is available at the stator. The frequency of the stator is the slip frequency and that of the rotor is the supply frequency [15]. The main application of the DFIG in wind plants is to generate power (power sent to the grid) in all three modes: sub synchronous, synchronous, and super synchronous. In this study, a DC shunt motor is used instead of a wind turbine to rotate the rotor. The DC shunt motor was controlled using a chopper drive [16]. In this study, we designed the DFIG to act as a motor at a speed below 560 rpm and a speed above 560 rpm to act as a generator. We considered a reference power of 422 W fed back to the grid through the stator. The grid-side converter (GSC) consumes power from the grid to generate power at the stator of the DFIG [17]. In addition, a phase-locked loop (PLL)-based park-transformation technique was designed to generate the reference signal required for the PWM techniques of both the grid-side and rotor-side converters of a doubly fed induction generator of a wind emulator. In the sub synchronous and synchronous modes of speed operation, the power fed back to the grid through the stator only, but in the super-synchronous mode, the power fed back to the grid through both the stator and rotor and the parameters of the slip ring induction motor, back-to-back converter, and shunt motor is given in Table 3,4, and 5.

Table.4. Parameters of DC shunt motor

Parameter Variable	Value
Output Power	2 H.P
Rated armature voltage	220V
Rated armature current	8A
Rated field voltage	220V
Rated field current	0.7A
Speed	1500 rpm

Table.5. Parameters of Slip ring induction motor

Parameter Variable	Value
Output Power	2 H.P
Stator voltage	415V
Stator current	3.5A
Rotor voltage	415V
Rotor current	3.5A
Speed	1440 rpm
Frequency	50Hz

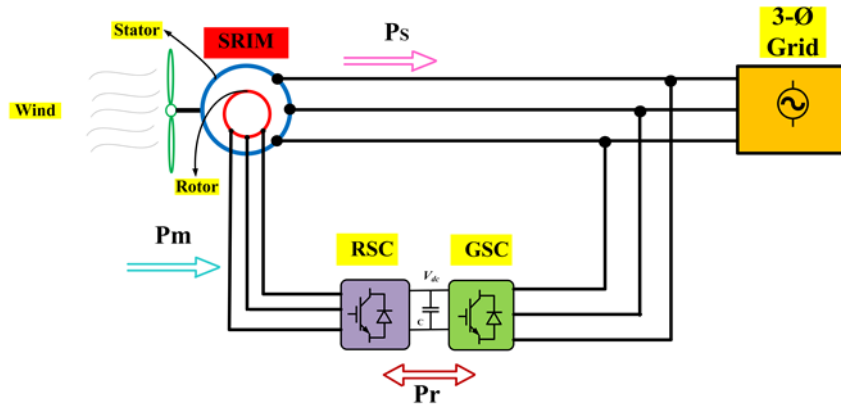


Fig.3. Basic circuit diagram of DFIG

IV. OPTIMIZATION ALGORITHMS

In this study, MPPT algorithms perturb and observe (P&O), and incremental conductance is used for the maximum power tracking of a solar panel. A field-programmable gate array controller was used in the grid-connected PV system to sense the voltage and current of the PV panel from the sensors and to compare them with the actual reference values. The necessary action was performed in the form of a gate pulse applied to the IGBT/MOSFET of the boost converter. MPPT algorithms were implemented using an FPGA SPARTAN6 controller. SP6 is an easy-to-use FPGA development board featuring a Xilinx Spartan-6 FPGA [18,19]. It was specifically designed for experimentation and research using a field-programmable gate array (FPGA). This development board features a Xilinx XC6SLX9 FPGA, with a maximum of 100 IOs.

A. Perturb and Observe Algorithm

Panel tracking involves placing a panel on a mount following the sun. It optimizes the output by following the sun across the sky to maximize the sunlight. This usually results in a 15% increase in winter and a 35% increase in summer [20]. The MPPT uses electronic tracking, which is typically digital. The controller looks at the output of the panel and compares it with the actual output [21]. You usually obtain a power increase of 20%-45% in summer and 10-15% in winter. Actual benefits can vary depending on the weather, temperature, battery conditions, and other factors. The tie-grid system has become popular because the price of the sun drops and electricity rates increase. Several brands of grid ties (i.e., no batteries) are available. All of these were built on MPPT [22].

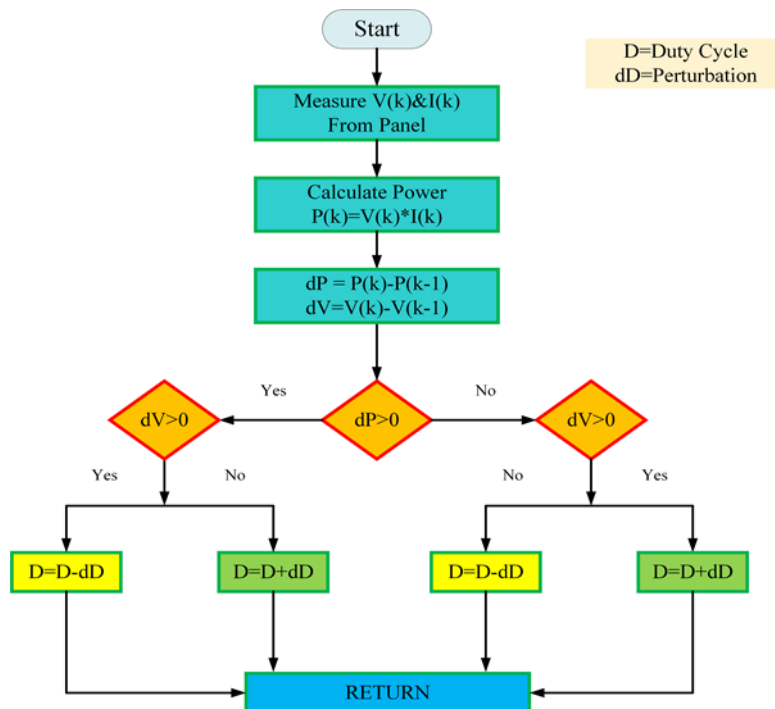


Fig.5. Flowchart of Perturb & Observe MPPT

**Description:** The MPPT technique was used in the PV system to maximize the output power by tracking the continuous maximum temperature of the panel and irradiance representation of the P&O flow graphics, as shown in Fig.5.

**STEP: 1** Measuring Voltage and Current: In this step, the voltage and current of the solar panel were measured, and the reference values of the voltage and current were set to a certain value.

**STEP: 2** Estimation of Power: In this step, the power of the solar panel was estimated by multiplying the measured voltage and current.

**STEP: 3** Difference with a reference value: In this step, the voltage and power value differences from the reference value represent the estimated duty cycles of the MOSFET and the IGBT, respectively.

**STEP: 4** Differentiation of Power: In this step, two steps are executed based on the differentiated value of power [23,24]. If the power differentiation is less than zero and if the voltage differentiation is less than zero, the duty cycle difference and addition are applied to the gate pulse of the MOSFET/IGBT.

*B. Incremental Conductance Algorithm*

This method uses the current derivative slope relative to the voltage required to reach the maximum power point [25]. The PV array must be adjusted to operate at the maximum value. Maximum power point tracking algorithms, such as the method of mining observations and incremental conductance, have been developed and are widely used in systems. The incremental conductance flow diagram is shown in Fig.6. The perturbation and observation method was adopted in this study for the PV array because of its simplicity and accuracy. The algorithm begins by selecting the initial reference voltage for the PV array [26]. The output powers of the two systems were then measured. If this power is not below the maximum strength, the initial reference value increases or decreases in one step [27].

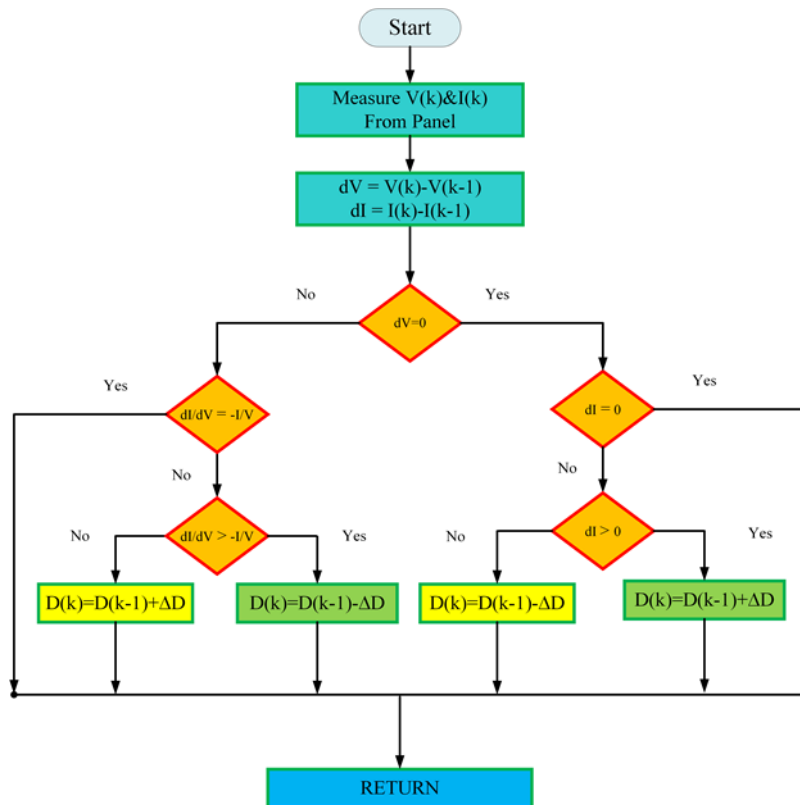


Fig.6. Flowchart of Incremental Conductance MPPT.

*C. Current Control Technique*

The harmonic distortion of the grid current can be reduced using a current control technique incorporated in a voltage-source converter [28]. The reference compensator current is obtained by subtracting the reference supply current from the grid current, as shown in Fig.7. The PWM current controller signal was obtained by subtracting the reference compensator current from the sensed compensator current. From the output of the pulse width modulation (PWM) current controller, that is, switching signals given to the firing angle of the voltage source converter, in the grid-connected PV-Wind hybrid system, no shunt active filter is used for harmonic reduction; however, the technique of current control is implemented to generate the firing angle of a VSC to reduce the total harmonic distortion of the grid current [29,30].

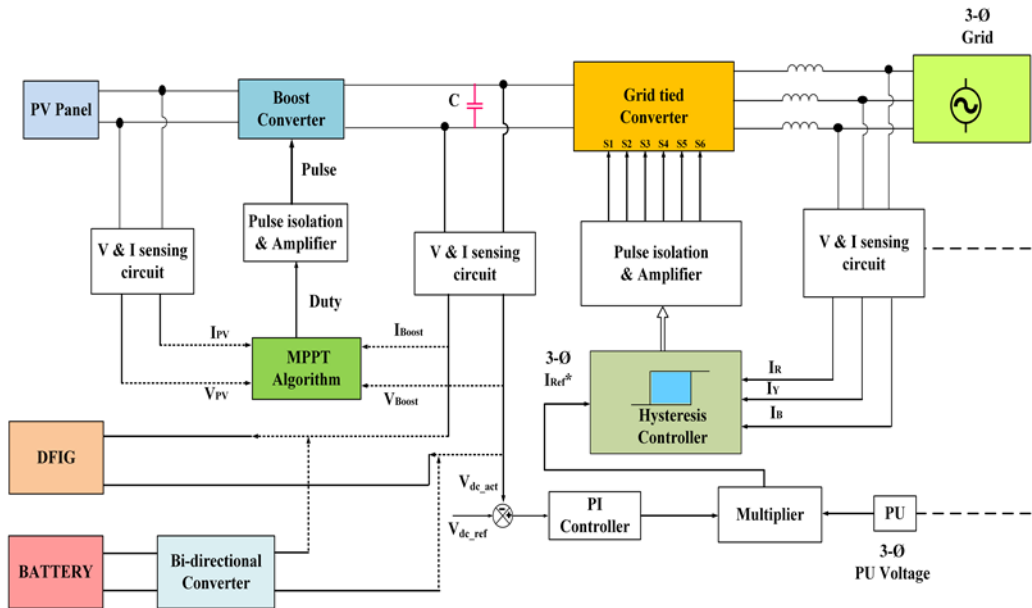


Fig.7 Block diagram of current control technique

V. EXPERIMENTAL RESULTS

The proposed block diagram of the PV-wind hybrid system is associated with a grid through a DC-DC boost converter and battery with a bidirectional buck-boost converter and 3-phase VSC, DFIG, as shown in Fig.8. MPPT was implemented in a boost converter with an FPGA controller in the hardware. The hardware model consisted of (a) a PV array with 1 kW at 1000 W/m<sup>2</sup> irradiance, (b) boost converter, (c) battery with buck-boost bidirectional converter, (e) DFIG with chopper circuit-fed DC drive control,(d) 3 phase VSC 10 kVA, and(e) three-phase autotransformer as a utility grid. The parameters of the buck-boost converter are listed in Table 6. The parameters of the voltage source converter and battery are listed in Tables 7 and 8, respectively.

Table 6. Parameters of Buck-Boost Converter.

Parameter Variable	Value
Output Power	2000W
Input Voltage Range DC(Min)	150V
O/P voltage range DC (Max)	350V
Switching Frequency up to	100KHz
Inductor(L2)	5mH
Capacitors(C3&C4)	1500µF
IGBT	1200V/100A

The hardware model used in this research was tested under different conditions.

- Performance analysis of DFIG power generation for all three-speed modes of operation.
- Power management strategy for the proposed hybrid system using P&O and INC algorithms under different load conditions.
- Improvement of the THD in the grid current using the current control technique employed in a VSC on the grid side.

Table 7. Parameters of Voltage Source Converter (VSC).

Parameter Variable	Value
Output Power	10KVA
Input DC Link Voltage	350V
DC Link Capacitor	660µF/450Vdc
Switching Frequency up to	100KHz
Output Frequency	10-50Hz
Load Current	15A Peak
IGBT	1200V/100A

Table 8. Battery Specifications

Parameter Variable	Value
Voltage	12V
Capacity	26Ah
No. of. batteries	12
Type	MF-VRLA

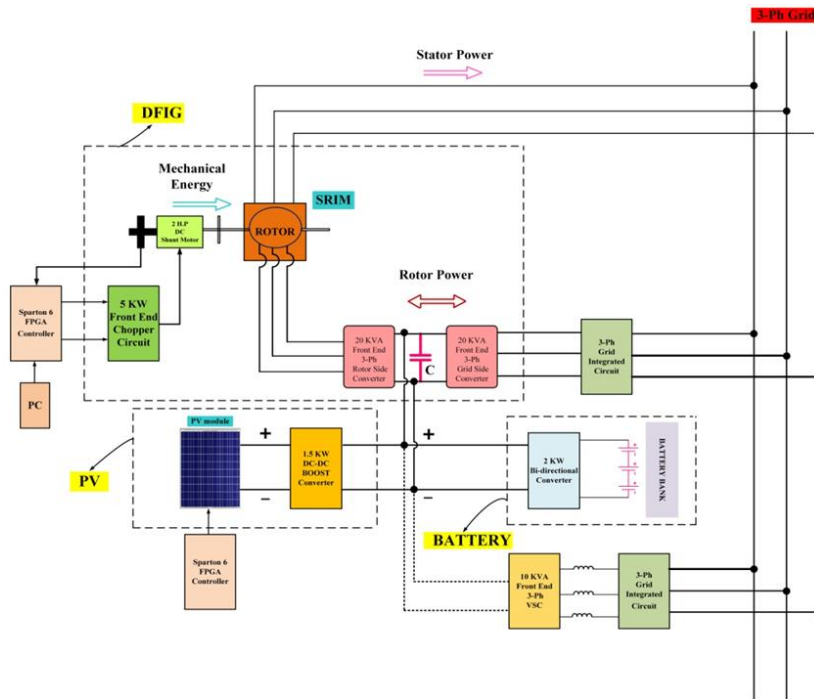
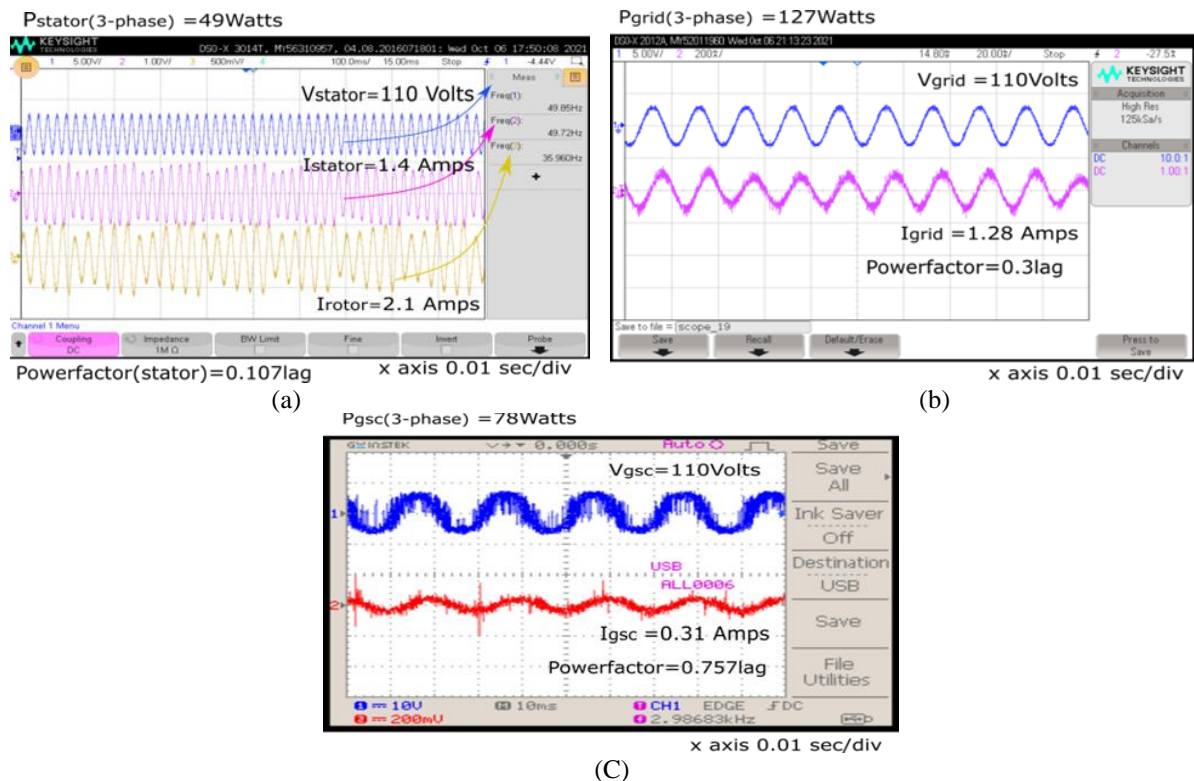


Fig.8. Proposed PV-wind hybrid system block diagram

A. *Performance analysis of power generation of DFIG alone at all three-speed modes of operation.*  
 Under this condition, we consider the DFIG alone for power generation at different speed modes of operation, as well as the power generated by the DFIG based on the reference power setting. Fig.9 (a), (b), and (c) indicate that the DFIG acts as an induction motor at a speed of less than 560 rpm in the proposed system. Therefore, it is tested one of the conditions for a motor speed of 400 rpm, under which the power available at the grid is equal to the sum of the power available at the stator and the power consumed by the grid-side converter from the grid. The power consumed by the grid-side converter was 78 W, the power consumed by the stator was +49 W (positive sign indicates power consumed from the grid), and the total power supplied by the grid was 127 W.



(C)  
 Fig.9. DFIG acting as a motor at a speed of 400 rpm corresponding the power-sharing between  
 (a) Stator (b) Grid (c) Grid side converter

Fig.10 (a), (b), and (c) indicate that the DFIG acts as a generator, and the power generation of the DFIG at a sub synchronous speed of 1200 rpm, where the power available at the grid is equal to the sum of the power delivered by the stator to the grid and the power consumed by the grid-side converter from the grid. The power consumed by the grid-side converter was 145 W, the power delivered by the stator was -419 W (the negative sign indicates the power delivered to the grid), and the total power available at the grid is 274 W.

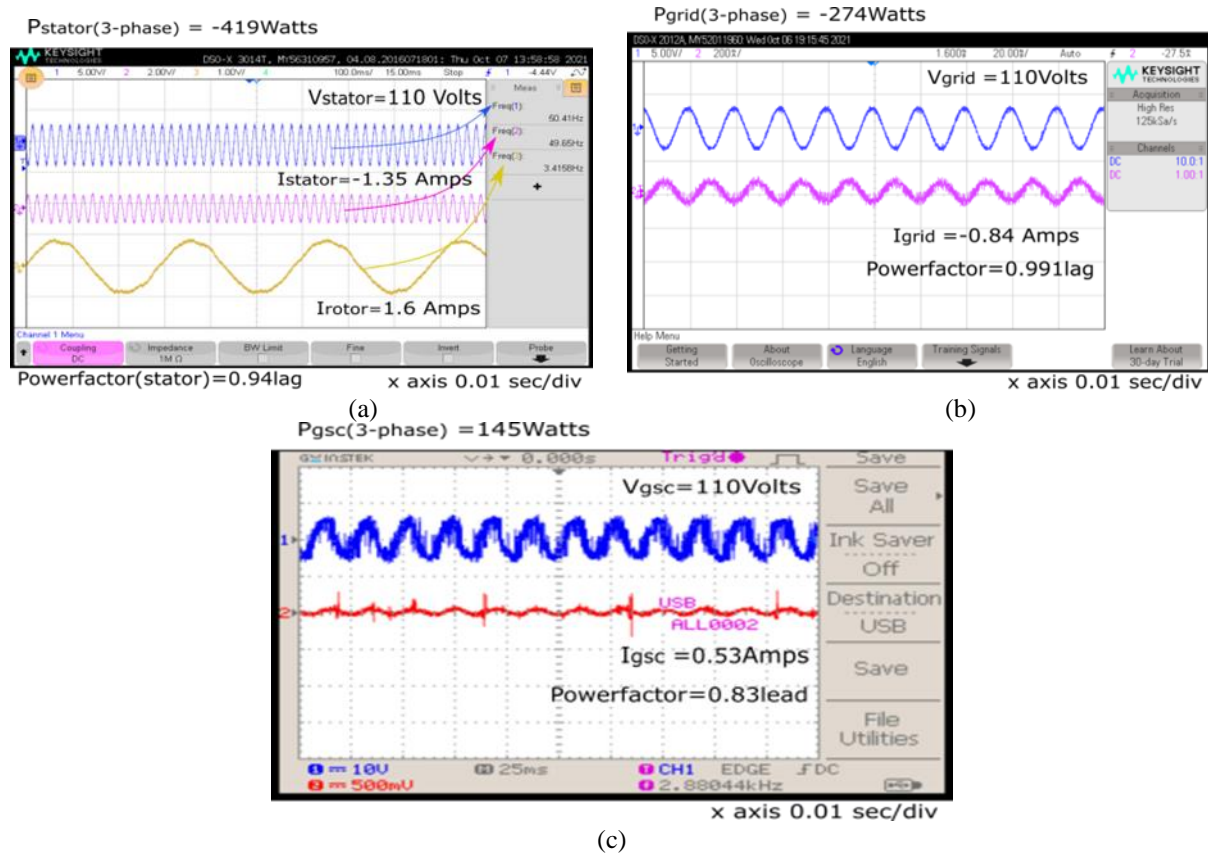


Fig.10. DFIG acting as a generator at sub synchronous speed of 1200 rpm corresponding to the power-sharing between (a) Stator (b) Grid (c) Grid side converter

Fig.12 (a), (b), and (c) indicate that the DFIG acts as a generator, and the power generation of the DFIG at a super synchronous speed of 1600 rpm, where the power available at the grid is equal to the sum of the power delivered by the stator to the grid and the power consumed by the grid-side converter from the grid, the power consumed by the grid-side converter is 78 W, the power delivered by the stator is -419 W ( the negative sign indicates power delivered to the grid), and the total power available at the grid is -340 W.

From the above performance analysis of the DFIG, we observed that the grid-side converter consumes less active power when the speed increases above the synchronous speed to generate same stator power (reference power) of 422 W to fed back to the grid, as shown in Table 9.

*B. Power management strategies of both P&O and incremental conductance MPPT algorithms at different load conditions at irradiance varying from 1000 W/m<sup>2</sup> to 700 W/m<sup>2</sup> and 25oc, and different DFIG speeds for the grid-connected hybrid system.*

Fig.13 (a), (b), and (c) show the power management strategy for a load demand of 1440 W using the incremental conductance MPPT algorithm. The total load demand of 1440 W supplied by the PV system was 551 W, the power supplied by the DFIG was -419 W, the power supplied by the battery was 52 W, and the power supplied by the grid was 418 W. Under these conditions, the battery delivered power to the load, that is, the discharging condition, and the DFIG delivered power to the load at a speed of 1200 rpm, as indicated by the negative sign.

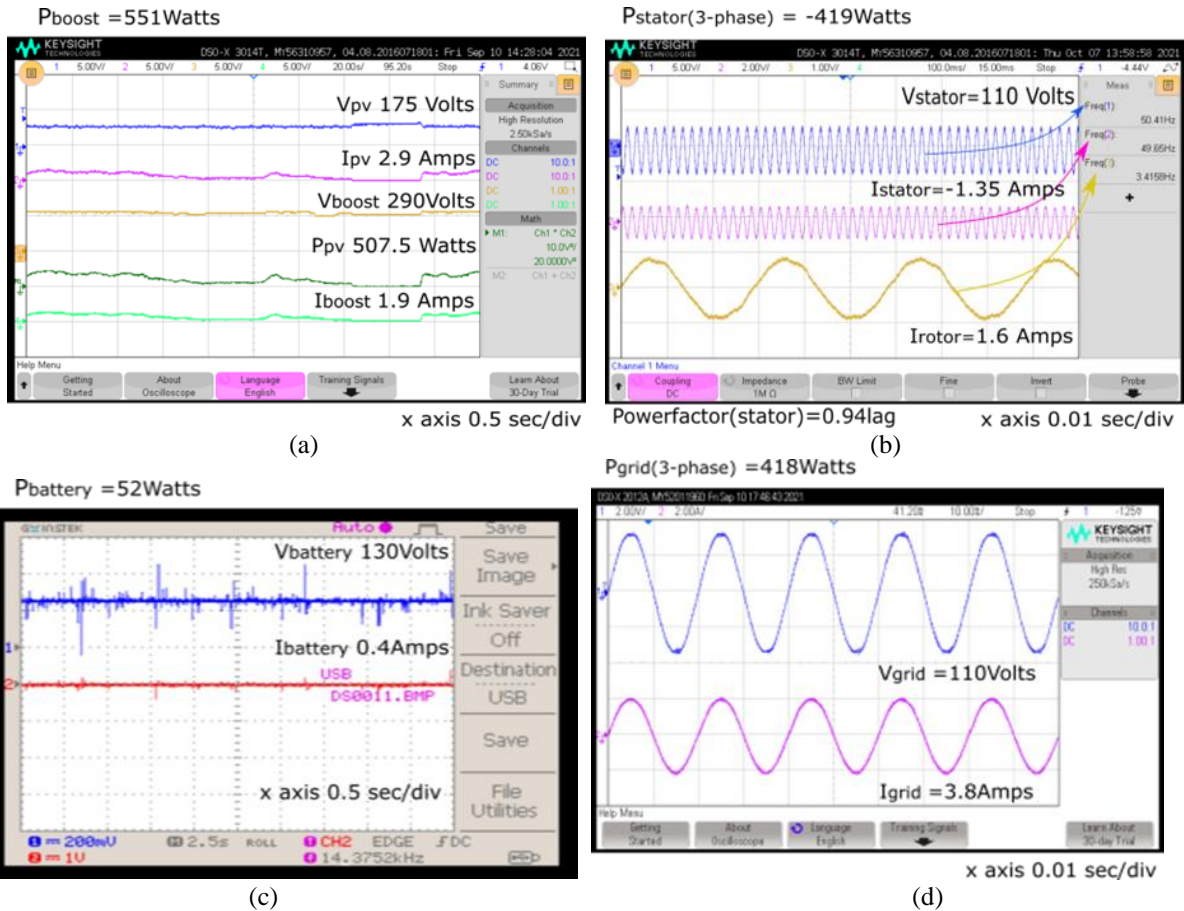
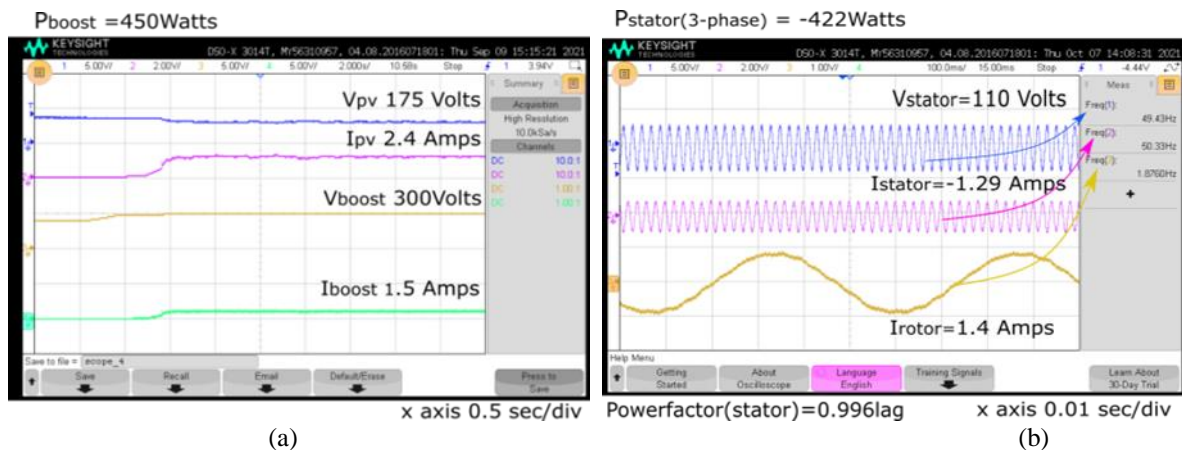


Fig.13. Power management strategy for a load of 1440watts with Incremental Conductance MPPT algorithm  
 (a) PV system (b) DFIG (c) Grid (d) Battery

Fig.14 (a), (b), and (c) show the power management strategy for a load demand of 820 W using the P&O MPPT algorithm. The total load demand of 820 W supplied by the PV system was 450 W, and the power supplied by the DFIG was -422 W; however, the load demand was 820 W; therefore, the excessive power delivered to the battery was -52 W. This negative sign indicates battery-consuming power from the PV system, that is, the charging condition, and the DFIG delivers power to the load at a speed of 1440 rpm, which is shown by the negative sign. Under these conditions, neither the grid is supplied nor consumed by the hybrid system.



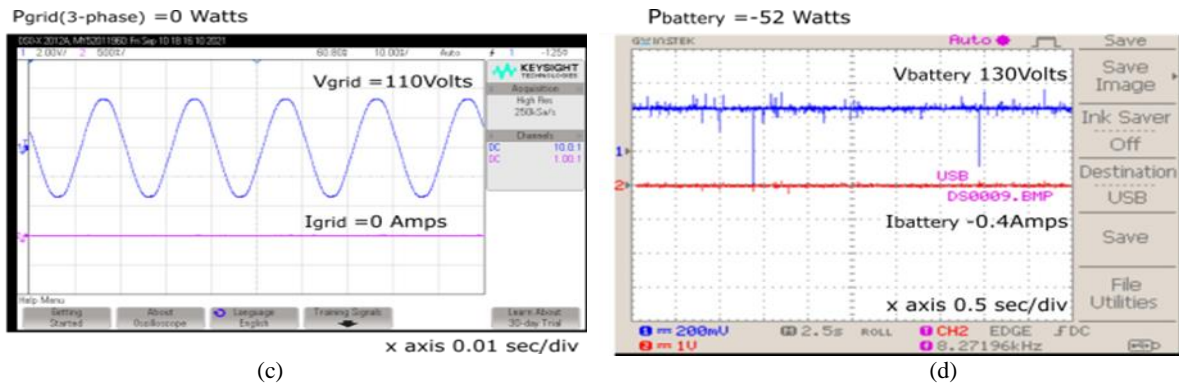


Fig.14. Power management strategy for a load of 820 watts with P&O MPPT algorithm  
 (a) PV system (b) DFIG (c) Grid (d) Battery

C. Improvement of THD in grid current by using current control technique employed in a voltage source converter (VSC) of the grid side.

Fig.16 (a) shows that the total harmonic distortion (THD) of the grid current without current control technique implemented in the firing angle of the voltage source converter at a constant load of 1440 W was 30.9%. Fig.16(b) shows that the total harmonic distortion of the grid current without current control technique implemented in the firing angle of the voltage source converter at a constant load of 720 W was 30.5%. Fig.16(c) shows that the total harmonic distortion of the grid current without current control technique implemented in the firing angle of the voltage source converter at a constant load of 480 W was 27.1%.

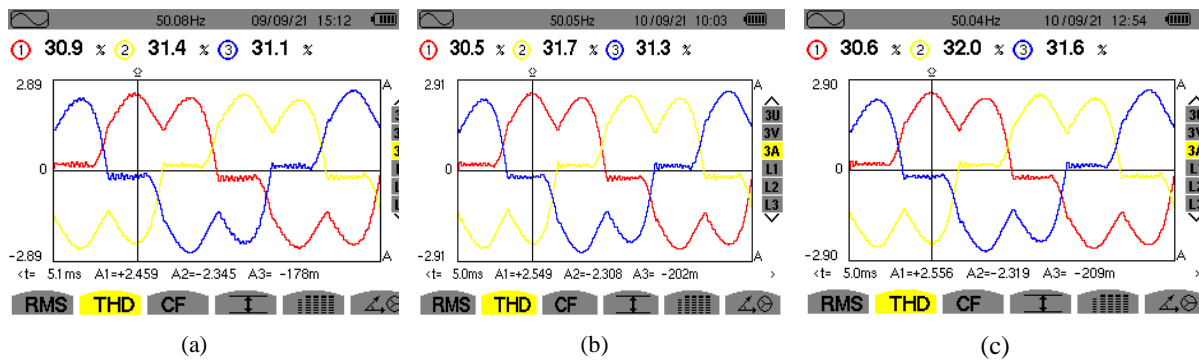


Fig.16. Grid Current Harmonic Analysis with different loads without current control technique in VSC  
 (a) 1440 watts (b) 720 watts (c) 480 watts

Fig.17 (a) shows that the total harmonic distortion of the grid current with current control technique implemented with INC MPPT at a constant load of 1440 W is 1.5%. Fig.17 (b) shows that the total harmonic distortion of the grid current with current control technique implemented with INC MPPT at a constant load of 720 W is 0.9%. Fig.17(c) shows that the total harmonic distortion of the grid current with current control technique implemented with INC MPPT at a constant load of 480 W is 0.7%.

The experimental setup for the grid-connected solar PV-wind hybrid system is shown in Fig.18. A THD comparison of the grid current for different loads is presented in Table.10. Figure 18 (a) shows the percentage (%) of current harmonics up to 50th order harmonics for a load of 480 watts without current control technique, Figure 18 (b) shows the percentage (%) of current harmonics up to 50th order harmonics for a load of 480 watts with current control technique of INC MPPT. and the power management strategies for the grid-connected hybrid systems for different loads are presented in Table 11.

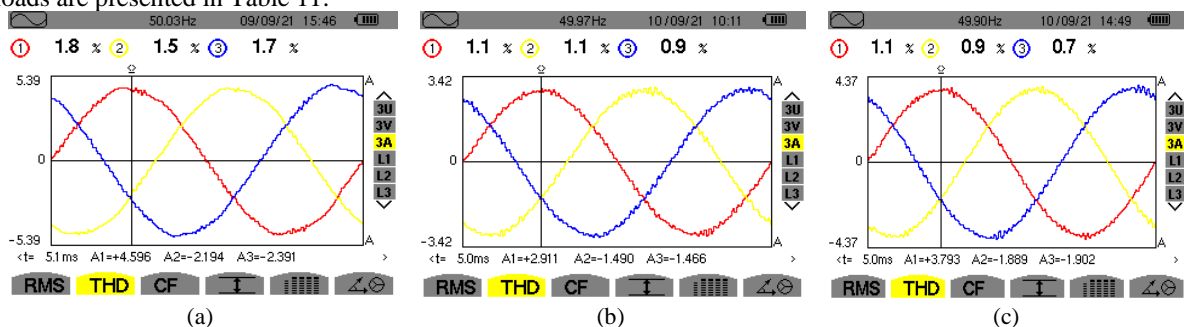


Fig.17. Grid Current Harmonic Analysis with different loads with current control technique with INC MPPT in VSC (a) 1440 watts (b) 720 watts (c) 480 watts

Table 10. THD Comparison of grid current for different loads

LOAD (Watts)	%THD (Without current control technique)	%THD (With current control technique of P&O MPPT)	%THD (With current control technique of INC MPPT)
1440	30.9	1.9	1.5
720	30.5	1.5	0.9
480	30.6	1.7	0.7
1230	29.7	2.1	1.3

(a)			(b)		
H	(%)	H	(%)	H	(%)
H01	100.0	H18	0.1	H35	0.6
H02	1.4	H19	2.1	H36	0.0
H03	3.6	H20	0.2	H37	1.2
H04	0.7	H21	0.3	H38	0.1
H05	47.2	H22	0.0	H39	0.3
H06	0.2	H23	1.7	H40	0.1
H07	20.4	H24	0.1	H41	0.4
H08	0.5	H25	1.6	H42	0.2
H09	0.9	H26	0.1	H43	0.7
H10	0.1	H27	0.5	H44	0.2
H11	7.3	H28	0.1	H45	0.5
H12	0.1	H29	0.8	H46	0.1
H13	4.1	H30	0.1	H47	0.5
H14	0.2	H31	1.0	H48	0.3
H15	0.3	H32	0.1	H49	0.7
H16	0.1	H33	0.6	H50	0.2
H17	3.1	H34	0.1		

Figure 18. Comparison of Percentage (%) of Current Harmonics up to 50<sup>th</sup> order harmonics for a load of 480 watt (a) without current control technique (b) with current control technique of INC MPPT

Table.11. Power management strategy for grid connected PV-wind hybrid system with an energy management for different loads

Load Demand (Watts)	MPPT Technique	PV(Watts)	WIND (Watts)	Grid (Watts)	Battery (Watts)
1440	INC	551	419	418	52
310	INC	522	415	-588	-39
480	INC	522	419	-419	-39
1230	P&O	475	419	300	38.8
820	P&O	450	422	0	-52
475	P&O	430	0	45	0

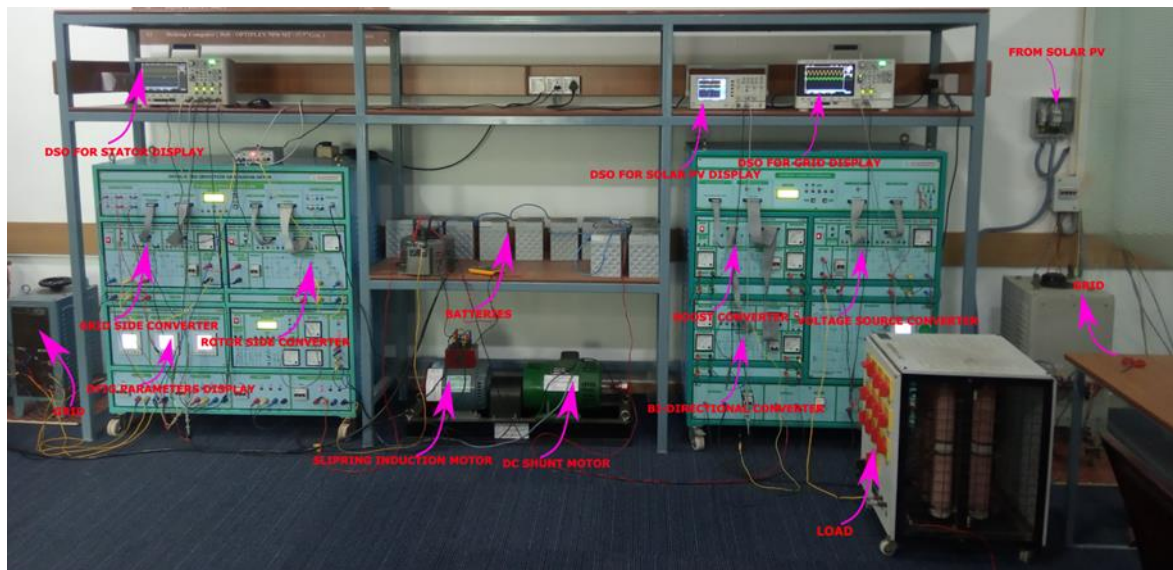


Fig.18. Experimental setup of the PV-wind hybrid system.

## VI. CONCLUSION

An MPPT-based hybrid system comprising PV, wind, and battery energy systems is implemented in this study. An MPPT-based closed-loop system is designed to control the boost converter. This study proposed P&O and INC MPPT controllers. A PLL-based park-transformation technique was designed to generate the reference signal required for the PWM techniques of both the grid-side and rotor-side converters of a doubly fed induction generator of a wind emulator. The bidirectional controller used for battery systems helps control the charging and discharging conditions of the battery. An FPGA based MPPT technique was implemented to set up the hardware implementation of the PV-wind and battery energy-based hybrid systems. A comparative analysis of the power management strategies of different MPPT techniques was performed. These results indicate that the INC MPPT technique yields better results than other MPPT controllers. The performance of the DFIG-based wind emulator is verified at different speeds. The THD in the grid current is improved with current control technique with INC MPPT as compared to the P&O MPPT technique.

## REFERENCES

- [1] Abir Muhtadi, et.al., "Renewable Energy based Microgrid: Role of the Architecture in Grid Enhancement towards Sustainable Energy" IEEE Industry Applications Society Annual Meeting, IEEE, 2020.
- [2] Alpernabiakpola, et.al., "Design Implementation and Operation of an Education Laboratory-Scale Microgrid" IEEE Access, 2021.
- [3] Caio Felipe Abe, et.al., "Computing Solar Irradiance and Average Temperature of Photovoltaic Modules From the Maximum Power Point Coordinates" IEEE Industry Applications Society Annual Meeting, IEEE, 2020.
- [4] Amjad Ali, et.al., "Investigation of MPPT techniques under uniform and non-uniform solar irradiation condition—a retrospection." Volume-8: 127368-127392, IEEE Access, 2020.
- [5] Pawel Rogowski, et.al., "Design and Implementation of Low-Cost Safety system for Small Wind Turbine" International Energy Conference (ENERGYCon), IEEE, 2020.
- [6] B. Srikanth Goud, et.al., "Optimization Techniques in PV-Wind based Distribution Generation- A Brief Review" 17th India Council International Conference (INDICON), IEEE, 2020.
- [7] Ratnakar Babu Bollipo, et.al., "Hybrid, Optimal, Intelligent and Classical PV MPPT Techniques: A Review" Journal of Power and Energy Systems, IEEE, 2021.
- [8] Abdallah Aldosary, et.al., "A modified shuffled frog algorithm to improve MPPT controller in PV System with storage batteries under variable atmospheric conditions," Control Engineering Practice, Elsevier, 2021. <https://doi.org/10.1016/j.conengprac.2021.104831>.
- [9] Amit kumar yadav, et.al., "Case Study of Grid-Connected Photovoltaic Power System Installed at Monthly Optimum Tilt Angles for Different Climatic Zones in India" IEEE Access, 2021.
- [10] Ankit Pal, et.al., "Performance Analysis of A Standalone PV System Under Dynamic Weather and Loading Conditions- A Case Study" Fourth International Conference on Inventive Systems and Control (ICISC), IEEE, 2020.
- [11] K. Umadevi, et.al., "Design and implementation of novel soft switching method based DC-DC converter with non-isolated coupled inductor in solar system using FPGA" Microprocessors and Microsystems, Elsevier, 2020. <https://doi.org/10.1016/j.micpro.2019.102952>.
- [12] Chinmay Das, et.al., "Design of PV Emulator Fed MPPT Controlled DC-DC Boost Converter for Battery Charging" First International Conference on Smart Technologies for Power, Energy and Control (STPEC), IEEE, 2020.
- [13] S. Raghavendran, et.al., "An Improved Three-level DC-DC Boost Converter for Renewable energy Systems with High Gain" 3rd International Conference on Energy, Power and Environment: Towards Clean Energy Technologies, IEEE, 2021.

- [14] Mohammed Fdaili, et al., "Control Strategies for DFIG-based Wind Turbine Systems Contributing to LVRT improvement and Grid Primary Frequency Adjustment" International Conference on Electrical and Information Technologies (ICEIT), IEEE, 2020.
- [15] Sambasivaiah Puchalapalli, et al., "A Micro grid Based on Wind-Driven DFIG, DG, and Solar PV Array for Optimal Fuel Consumption" IEEE Transactions on Industry Applications, IEEE, 2020.
- [16] José Antonio Cortajarena, et al., "Grid Frequency and Amplitude Control Using DFIG Wind Turbines in a Smart Grid" Mathematics, MDPI, 2020.
- [17] MdAktarujjaman, et al., "Impact of DFIG Based Wind Generation on Grid Voltage and Frequency Support" International Symposium on Power Electronics, Electrical Drives, Automation and Motion (SPEEDAM), IEEE, 2020.
- [18] A.Senthilvel, et al., "FPGA based implementation of MPPT algorithms for photovoltaic system under partial shading conditions" Microprocessors and Microsystems, Elsevier, 2020. <https://doi.org/10.1016/j.micpro.2020.103011>.
- [19] Mohamed Yassine Allani, et al., "FPGA-Based Controller for a Hybrid Grid-Connected PV/Wind/Battery Power System with AC Load" Energies, MDPI, 2021.
- [20] Vishakha, et al., "Review of Optimization Techniques for Hybrid Wind PV-ESS System" International Conference on Power Electronics & IoT Applications in Renewable Energy and its Control (PARC), IEEE, 2020.
- [21] Hussaian Bash, CRani. "Different Conventional and Soft Computing MPPT Techniques for Solar PV systems with High Step-Up Boost Converters" A Comprehensive Analysis, Energies, 2020.
- [22] Md.Hanif Reza, et al., "Efficiency Evaluation of P&O MPPT Technique used for Maximum Power Extraction from Solar Photovoltaic System" Region 10 Symposium (TENSYP), IEEE, 2020.
- [23] Kwabena Owusu Sarfo, et al., "An Improved P&O MPPT Algorithm Under Partial Shading Conditions" IEEE PES/IAS PowerAfrica, IEEE, 2020.
- [24] Ashutosh Mohanty, et al., "Modified P&O MPPT Boost Converter and Voltage control Inverter based Island Solar PV with Power quality analysis under the varying load and changing weather condition" International Symposium on Sustainable Energy, Signal Processing and Cyber Security (ISSSC), IEEE, 2021.
- [25] Nathan Chris Swanepoel, et al., "Experimental Investigation of Incremental Conductance-based MPPT for PV Arrays" IEEE PES/IAS PowerAfrica, IEEE, 2020.
- [26] Satabdi Bhattacharya, et al., "Modified Incremental Conductance MPPT Algorithm for Very Fast Changing Atmospheric Condition for Solar Electric Vehicle Application" 16th India Council International Conference (INDICON), IEEE, 2020.
- [27] Dino Mustafić, et al., "Implementation of Incremental Conductance MPPT Algorithm in Real Time in Matlab/Simulink Environment with Humusoft MF634 Board" 9th Mediterranean Conference on Embedded Computing (MECO), IEEE, 2020.
- [28] Stefan P. Engel, et al., "Instantaneous current control for the three-phase dual-active bridge DC-DC converter" Energy Conversion Congress and Exposition (ECCE), IEEE, 2021.
- [29] Rayane Mourouvin, et al., "Understanding the role of VSC control strategies in the limits of power electronics integration in AC grids using modal analysis" Electric Power Systems Research, Elsevier, 2021. <https://doi.org/10.1016/j.epsr.2020.106930>.
- [30] Rui Yin, et al., "Modeling and stability analysis of grid-tied VSC considering the impact of voltage feed-forward" International Journal of Electrical Power & Energy Systems, Elsevier, 2021. <https://doi.org/10.1016/j.ijepes.2021.107483>.